Constraint on the solar Δm^2 using 4000 days of short baseline reactor neutrino data

Alvaro Hernandez Cabezudo[†]
Institut für Kernphysik, Karlsruher Institut für Technologie (KIT), D-76021 Karlsruhe, Germany

Stephen J. Parke[‡]
Theoretical Physics Department, Fermi National Accelerator Laboratory, Batavia, Illinois 60510, USA

Seon-Hee Seo[*]
Center for Underground Physics, Institute for Basic Science, Daejeon 34126, Korea

(Received 16 August 2019; published 20 December 2019)

There is a well-known 2σ tension in the measurements of the solar Δm^2 between KamLAND and SNO/Super-KamioKANDE. Precise determination of the solar Δm^2 is especially important in connection with current and future long baseline *CP* violation measurements. Seo and Parke [Phys. Rev. D **99**, 033012 (2019)] points out that currently running short baseline reactor neutrino experiments, Daya Bay and RENO, can also constrain solar Δm^2 value as demonstrated by a GLoBES simulation with a limited systematic uncertainty consideration. In this work, the publicly available data, from Daya Bay (1958 days) and RENO (2200 days) are used to constrain the solar Δm^2. Verification of our method through Δm^2_{ee} and $\sin^2\theta_{13}$ measurements is discussed in Appendix A. Using this verified method, reasonable constraints on the solar Δm^2 are obtained using above Daya Bay and RENO data, both individually and combined. We find that the combined data of Daya Bay and RENO set an upper limit on the solar Δm^2 of 18×10^{-5} eV^2 at the 95% C.L., including both systematic and statistical uncertainties. This constraint is slightly more than twice the KamLAND value. As this combined result is still statistics limited, even though driven by Daya Bay data, the constraint will improve with the additional running of this experiment.

DOI: 10.1103/PhysRevD.100.113008

I. INTRODUCTION

Evidence that neutrinos are massive and mix is well established by a significant number of experiments. In this paper, we are interested in the mass squared difference, Δm^2_{21}; the mass squared difference of the two mass eigenstates that have the greatest fraction of electron neutrino, ν_1 and ν_2. This mass splitting is responsible for the neutrino flavor transformations that occur inside the Sun (hence the name the solar mass squared difference), and for the antineutrino oscillations observed at an L/E $\sim$ 15 km/MeV.

In this paper, we use publicly available data to follow up a recent paper [1], that Daya Bay [2] and RENO [3], the short baseline ($\sim$1.5 km) reactor antineutrino experiments currently running, have enough data already collected to constrain Δm^2_{21}.

The combined constraint by Daya Bay and RENO, gives an important consistency check of the standard three neutrino paradigm as well as adding addition information to the size of Δm^2_{21}. The $\sim 2\sigma$ tension between the combined Super-Kamiokande (SK) [4] & Sudbury Neutrino Observatory (SNO) [5] solar neutrino measurements and KamLAND [6] reactor experiment ($L/E \sim 50$ km/MeV) is not directly addressed by this constraint. However such a combined Daya Bay plus RENO constraint is at a different L/E range ($\sim$0.5 km/MeV) than the above mentioned measurements as well as JUNO [7]. Moreover, the ratio of Δm^2_{21} to Δm^2_{31}, at an $L/E \sim 0.5$ km/MeV, is required for the precision measurement of leptonic *CP* violation parameter, by NOvA [8], T2K [9] and future Long Baseline (LBL) experiments.

Currently there are two measurements of the solar mass squared difference, Δm^2_{21}. One measurement comes from a

[*]Corresponding author.
sunny.seo@ibs.re.kr
[†]alvaro.cabezudo@kit.edu
[‡]parke@fnal.gov

combined measurement by SNO and SK using the observation of a day-night asymmetry by SK and the nonobservation of the low energy up turn of the ^{8}B neutrino survival probability by SNO and SK. This combined result is

$$\Delta m^2_{21} = 5.1^{+1.3}_{-1.0} \times 10^{-5}\ \text{eV}^2, \quad (1)$$

from SNO and SK. Similar results are obtained by Nu-Fit [10]. The other measurement is from KamLAND, the long baseline reactor antineutrino experiment, see [6], at

$$\Delta m^2_{21} = 7.50^{+0.20}_{-0.20} \times 10^{-5}\ \text{eV}^2, \quad (2)$$

If CPT invariance is a good symmetry of nature then the Δm^2_{21} measured from solar neutrinos and reactor antineutrinos is required to give the same value. Currently this important parameter for neutrino physics suffers from a 2σ level tension. This tension could come from new physics, some error in the analysis of one or more of the experiments or a statistical fluctuation.

Moreover, the ratio of Δm^2_{21} to Δm^2_{31} is required for the determination of the CP phase, δ, in the long baseline neutrino[1] oscillation experiments (NOvA, DUNE [11], T2K, T2HK [12], T2HKK [13]) as the size of the CP violation is proportional to Δm^2_{21} to Δm^2_{31}, as well as the Jarlskog invariant. At $L/E \sim 500$ km/GeV $=$ 0.5 km/MeV, the first oscillation peak in vacuum, for $\nu_\mu \to \nu_e$

$$P(\bar{\nu}_\mu \to \bar{\nu}_e) - P(\nu_\mu \to \nu_e) \approx \pi J \left(\frac{\Delta m^2_{21}}{\Delta m^2_{31}}\right) \quad (3)$$

where the Jarlskog invariant, J, is $J = \sin 2\theta_{12} \sin 2\theta_{13} \cos\theta_{13} \sin 2\theta_{23} \sin\delta \approx 0.3 \sin\delta$.

In the bievent plane for T2K, see Fig 44 of [14],

$$N(\nu_\mu \to \nu_e) = 37 \quad \text{and} \quad N(\bar{\nu}_\mu \to \bar{\nu}_e) = 4$$

is outside the allowed region (by about 1σ). This can be well accommodated by a Δm^2_{21} value, approximately twice the KamLAND value. Again, this is probably a statistical fluctuation but with only the KamLAND precision measurement of Δm^2_{21}, other possibilities are still viable.

The future medium baseline, $L/E \sim 15$ km/MeV, reactor experiment JUNO will measure to better than 1% precision Δm^2_{21} and $\sin^2\theta_{12}$, see [7]. JUNO experiment is currently under construction and their precision measurements of Δm^2_{21} and $\sin^2\theta_{12}$ will not be available until approximately 5 years from now. Later next decade, the proposed experiments Hyper-K & DUNE will also give us precision measurements of Δm^2_{21} using ^{8}B solar neutrinos, see [15,16] respectively.

In Sec. II, we briefly discuss in detail the effects of increasing Δm^2_{21} on the $\bar{\nu}_e$ survival probability. Then in Sec. III Daya Bay and RENO data sets used in this work are discussed followed by Secs. IV, V, and VI for methods and systematic uncertainties, results, and conclusion, respectively.

II. SURVIVAL PROBABILITY

In vacuum, the electron antineutrino survival probability is

$$\begin{aligned} P(\bar{\nu}_e \to \bar{\nu}_e) &= 1 - P_{12} - P_{13} \quad \text{with} \\ P_{12} &= \sin^2 2\theta_{12} \cos^4\theta_{13} \sin^2\Delta_{21}, \\ P_{13} &= \sin^2 2\theta_{13} (\cos^2\theta_{12} \sin^2\Delta_{31} + \sin^2\theta_{12} \sin^2\Delta_{32}), \end{aligned} \quad (4)$$

where the kinematic phases are given by $\Delta_{jk} \equiv \Delta m^2_{jk} L/(4E)$ and $\theta_{13} \approx 8°$ and $\theta_{12} \approx 33°$ are the reactor and solar mixing angles respectively. The P_{12} term is associated with the solar oscillation scale of 15 km/MeV and the P_{13} term is associated with the atmospheric oscillation scale of 0.5 km/MeV. To excellent fractional precision,[2] the P_{13} term can be approximated by

$$P_{13} \approx \sin^2 2\theta_{13} \sin^2\Delta_{ee} \quad (5)$$

where $\Delta m^2_{ee} \equiv \cos^2\theta_{12} \Delta m^2_{31} + \sin^2\theta_{12} \Delta m^2_{32}$ [17,18], interpreted as the ν_e average of Δm^2_{31} and Δm^2_{32}.

Using the fit values given in [10], and an L/E range around the first oscillation minimum ($L/E \sim 0.5$ km/MeV), P_{12} and P_{13} is well approximated by:

$$P_{12} \approx 0.002 \left(\frac{L/E}{0.5\ \text{km/MeV}}\right)^2 \left(\frac{\Delta m^2_{21}}{7.5 \times 10^{-5}\ \text{eV}^2}\right)^2 \quad (6)$$

$$P_{13} \approx 0.08 \sin^2\left(\frac{\pi}{2}\left(\frac{L/E}{0.5\ \text{km/MeV}}\right)\right). \quad (7)$$

The P_{12} term is almost negligible for all $L/E < 1$ km/MeV, if $\Delta m^2_{21} = 7.5 \times 10^{-5}$ eV^2. For Daya Bay and RENO this covers the full L/E range.

Suppose that Δm^2_{21} is 3 times larger than KamLAND value, i.e., 22.5×10^{-5} eV^2, then

[1] In the rest of this paper, when referring to neutrinos, we mean both neutrinos and/or antineutrinos.

[2] The fractional precision is better than 0.05% for L/E < 1 km/MeV. Also, in this L/E range, the exact P_{13} is very insensitive to mass ordering provided the value of $|\Delta m^2_{ee}|$ is the same for both mass orderings.

TABLE I. Live days (not operational days), effective baseline distance (L_{eff}), observed IBD and background events for Daya Bay and RENO used in this work. For Daya Bay there are two near detectors in different sites.

	Daya Bay: Near	Daya Bay: Far	RENO: Near	RENO: Far
Live days	(1,637.12, 1,647.64)	1,692.69	1,807.88	2,193.04
L_{eff} (m)	(562.2, 594.2)	1637	430.4	1445.4
Total # of IBD events	(1,763,939, 1,651,088)	486,873	833,433	98,292
Total # of background events	(19,056, 13,634)	2,230	17,229	4,912

$$P_{12} \approx 0.02\left(\frac{L/E}{0.5\ \text{km/MeV}}\right)^2\left(\frac{\Delta m^2_{21}}{22.5\times 10^{-5}\ \text{eV}^2}\right)^2. \quad (8)$$

Now P_{12} is now no longer tiny compared to P_{13} at $L/E = 0.5$ km/MeV, oscillation minimum, and as L/E gets larger than 0.5 km/MeV, P_{12} gets bigger, whereas P_{13} is getting smaller. At an $L/E = 1$ km/MeV, P_{12} would be approximately equal to $\sin^2 2\theta_{13}$ (0.08) for this value of Δm^2_{21}. It is this quadratic rise in P_{12} as Δm^2_{21} increases that we exploit to place an upper limit on Δm^2_{21}. For further details on the survival probability as Δm^2_{21} increases see [1].

III. DAYA BAY AND RENO DATA SETS

In this work, 1958 days of Daya Bay data [19] and 2200 days of RENO data [20] are used, where Daya Bay has about five times more inverse beta decay (IBD) events than RENO in their far detectors. Daya Bay data including background estimation, energy response function, and systematic uncertainties are taken from the supplementary material in [19]. RENO data and background estimation are extracted from Fig. 1 in [20] and systematic uncertainties are also taken from [20]. Table I shows summary of the basic parameters, i.e., L_{eff}, IBD rate, and background rate, for near and far detectors of Daya Bay and RENO used in this analysis. Note that there are two near detectors in different sites for Daya Bay.

IV. METHODS AND SYSTEMATIC UNCERTAINTIES

Best fit values on Δm^2_{21} and $\sin^2 2\theta_{13}$ are obtained by finding minimum χ^2 values between data and predictions for all possible combination of the two parameters. Far-to-near ratio method is employed in this χ^2 analysis to avoid the spectral shape anomaly around 5 MeV region [21] as well as to reduce systematic uncertainties.

The χ^2 formalism as written below contains a covariance matrix ($V_{\text{stat},ij}$) to include statistical uncertainty and pull parameters (ξ_α) to include systematic uncertainties.

$$\chi^2 = \sum_{i,j}^{N_{\text{bins}}} (D_i^{F/N} - P_i^{F/N}) V^{-1}_{\text{stat},ij} (D_j^{F/N} - P_j^{F/N}) + \sum_{\alpha}^{N_{\text{pull}}} \frac{(\xi_\alpha - 1)^2}{\sigma_\alpha^2},$$

where, $D_i^{F/N} \equiv \frac{O_i^F - B_i^F}{O_i^N - B_i^N}$, $P_i^{F/N} \equiv \frac{X_i^F}{X_i^N}$, and $F(N)$ and i (j) represent the Far (Near) detector and ith (jth) prompt energy bin, respectively. Being O the observed number of IBD candidate events, B the estimated background number of events and X the expected number of events for a given Δm^2_{21} and $\sin^2 2\theta_{13}$ pair. A total of 26 energy bins (N_{bins}) is used for RENO from 1.2 to 8.4 MeV. The same number of energy bins are used for Daya Bay from 0.7 to 12 MeV but two near detectors are taken into account in the χ^2 formalism by replacing N_{bins} to $2N_{\text{bins}}$ where for $1 \le i \le N_{\text{bins}}$, $F = \text{EH3}$ and $N = \text{EH1}$, and for $\text{N}_{\text{bins}} + 1 \le i \le 2\text{N}_{\text{bins}}$, $F = \text{EH3}$ and $N = \text{EH2}$.

For both Daya Bay and RENO, systematic uncertainties on the relative detection efficiency, relative energy scale and the main background contributions are taken into account as summarized in Table II.

Besides the systematic uncertainties, additional systematic paddings (adjustment factors) are added in our work to match Daya Bay and RENO results on θ_{13} and Δm^2_{ee} measurements. For Daya Bay a 1.3 adjustment factor to the relative energy scale and Li-He background uncertainties is added. Whereas in RENO a 1.4 adjustment factor is added to the relative detection efficiency uncertainty. More details on the validation of our method and expected event description can be found in Appendixes A and B. The RENO predictions are computed using the Daya Bay detector response function and the relative far-to-near normalization is computed comparing our total number of expected events with the total number of expected events in the RENO Far detector. In order to match the best fit values of θ_{13} and Δm^2_{ee} a 0.984 adjustment factor is added to this normalization of a total event rate for RENO.

TABLE II. Relative systematic uncertainties used in this work for Daya Bay and RENO, taken from [19,20] respectively.

	Daya Bay	RENO
Source	Uncertainty %	
Detection efficiency	0.13	0.21
Energy scale	0.2	0.15
Li-He background	30	5–8
Fast neutron background	13–17	…
Accidental background	1	…

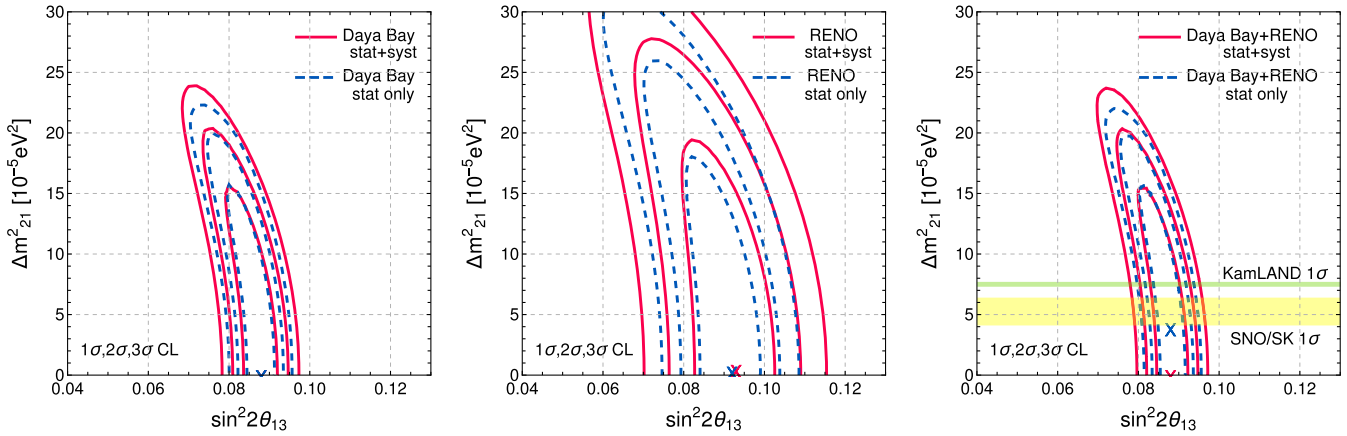

FIG. 1. The 1, 2 and 3σ allowed regions in the Δm^2_{21} vs $\sin^2 2\theta_{13}$ parameter space for Daya Bay (1958 days, 487 K IBD events at Far) (left panel) and RENO (2200 days, 98 K IBD events at Far) (middle panel) and the Daya Bay and RENO combined (right panel). In this fitting, the Δm^2_{ee} value is constrained using the value from current long baseline (LBL) neutrino experiments, see Eq. (9). In the right panel the KamLAND and SNO/SK 1σ bands are overlaid for comparison and this contour plot shows that this measurement is still statistics limited.

V. RESULTS

A 2-dimensional scan over Δm^2_{21} and $\sin^2 2\theta_{13}$ is performed to find the best fit value pair at the minimum value of χ^2 described earlier, where in the oscillation probability, the parameter θ_{12} is fixed[3] at $\sin^2\theta_{12}=0.310$. The Δm^2_{ee} parameter is constrained with a pull parameter, allowing it to vary within a 2σ range of a prior Δm^2_{ee} value with a penalizing term

$$\left(\frac{\Delta m^2_{ee,\text{prior}} - \Delta m^2_{ee}}{\sigma}\right)^2$$

The prior Δm^2_{ee} value and its uncertainty are taken to be

$$\Delta m^2_{ee} = 2.45 \pm 0.15 \times 10^{-3}\ \text{eV}^2 \tag{9}$$

which is inferred from the combined measurement on $\Delta m^2_{\mu\mu}$ by current long baseline neutrino experiments in [10] through $\Delta m^2_{ee} \simeq \Delta m^2_{\mu\mu} \pm \cos 2\theta_{12}\Delta m^2_{21}$, see [17], where the $+/-$ comes from the unknown mass ordering (NO/IO) and ignoring terms proportional to $\sin\theta_{13}\Delta m^2_{21}$. The unknown mass ordering is treated as an additional uncertainty (4%) to $\Delta m^2_{\mu\mu}$ uncertainty (4%) for the Δm^2_{ee} uncertainty which, therefore, becomes about 6%.

The best fit, 1, 2, and 3σ allowed regions of Δm^2_{21} vs $\sin^2 2\theta_{13}$ are shown in Fig. 1 with (solid lines) and without (dashed lines) systematic uncertainties for Daya Bay and RENO, separately and combined. Daya Bay's result is better than RENO's due to about five time more statistics at the far detector, see Table I.

[3]A discussion on the effects of varying θ_{12} in this analysis can be found in [1].

Figure 2 shows the χ^2 projection over Δm^2_{21}, obtained by minimizing over $\sin^2 2\theta_{13}$, for the Daya Bay plus RENO combined analysis. The upper bounds on Δm^2_{21}, including systematic uncertainties, are 12.3, 18.3 and 22.3×10^{-5} eV^2 at 1, 2 and 3σ CL, respectively. Current upper bounds are limited by statistics.

In Fig. 3, we give the constraints on the three parameter fit, Δm^2_{21}, Δm^2_{ee} and $\sin^2 2\theta_{13}$, without imposing any constrain on Δm^2_{ee}, using the combined Daya Bay and RENO data sets. Both statistical and systematic uncertainties are included in this plot. As before θ_{12} is fixed at $\sin^2\theta_{12} = 0.310$, see [1] for discussion on allowing $\sin 2\theta_{12}$ to also vary.

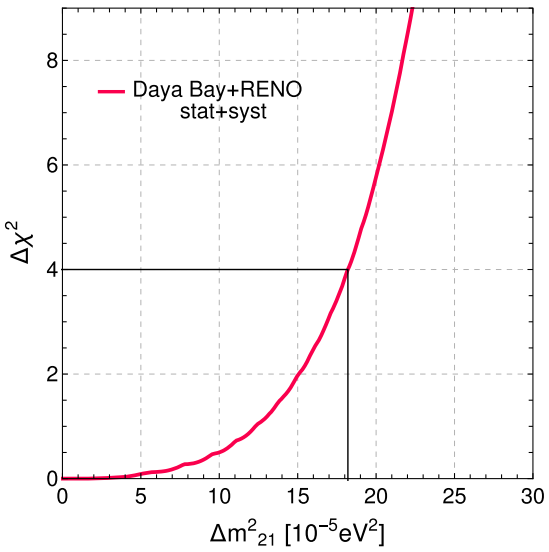

FIG. 2. The Daya Bay and RENO combined analysis for the $\Delta\chi^2$ projection of the Δm^2_{21} measurement including systematic uncertainty, minimizing over $\sin^2 2\theta_{13}$. At the 2σ (95%) C.L. Δm^2_{21} is constrained to be less than $18.3(18) \times 10^{-5}$ eV^2.

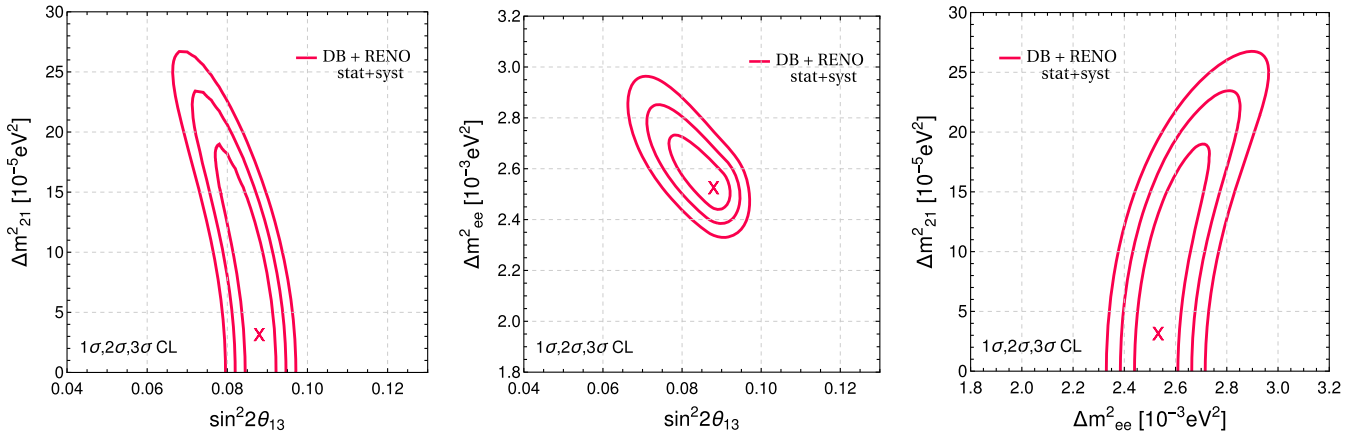

FIG. 3. Simultaneous three parameter fit for Δm^2_{21}, Δm^2_{ee} and $\sin^2 2\theta_{13}$ using the combined Daya Bay (1,958 days, 487 K IBD events at Far) and RENO (2,200 days, 98 K IBD events at Far) data. The best fit point is found at $\Delta m^2_{21} = 3.3 \times 10^{-5}$ eV^2, $\Delta m^2_{ee} = 2.5 \times 10^{-3}$ eV^2, $\sin^2 2\theta_{13} = 0.088$.

Results with Δm^2_{ee} fixed or free are obtained for each experiment and for when the data from both experiments are combined. These are described and given in Appendix C. It was found that the effect of free Δm^2_{ee} is bigger than that of systematic uncertainty, but our representing results are based on constrained Δm^2_{ee} since it is a reasonably well measured oscillation parameter using LBL experiments.

VI. CONCLUSION

Using the currently available public data from Daya Bay (1,958 days) and RENO (2,200 days), we have provided additional information on the solar Δm^2. A reasonable upper bound is obtained from a combined analysis of the Daya Bay and RENO data as 18×10^{-5} eV^2 at 95% CL, where Δm^2_{ee} was constrained using a pull parameter with input information from LBL experiments. Our combined analysis result is currently limited by statistics and, as expected, Daya Bay data drives the combined analysis results. Our analysis method was validated by reproducing the Δm^2_{ee} and $\sin^2\theta_{13}$ contours for each experiment as discussed in Appendix A.

Given that the previous measurements by KamLAND and SK/SNO of the solar Δm^2 are in a 2σ tension and the importance of solar Δm^2 for the determination of CP violation in LBL experiments, it is crucial that we understand the value of the solar Δm^2 better. It is expected by circa 2025 that the JUNO experiment will provide additional, important information on the value of the of solar Δm^2.

ACKNOWLEDGMENTS

We are grateful to Thomas Schwetz for fruitful discussions. This work (S. H. S.) was supported by the National Research Foundation of Korea (NRF) grant funded by the Korea Ministry of Science and ICT (MSIT) (No. 2017R1A2B 4012757 and IBS-R016-D1-2019-b01). This manuscript has been authored (S. J. P.) by Fermi Research Alliance, LLC under Contract No. DE-AC02-07CH11359 with the U.S. Department of Energy, Office of Science, Office of High Energy Physics. This project (S. J. P.) has received funding/support from the European Union's Horizon 2020 research and innovation programme under the Marie Sklodowska-Curie grant agreement No. 690575 & No. 674896.

APPENDIX A: VALIDATION OF OUR ANALYSES

Using the data and the χ^2 formalism described in Secs. III and IV, our method reproduces the contours in

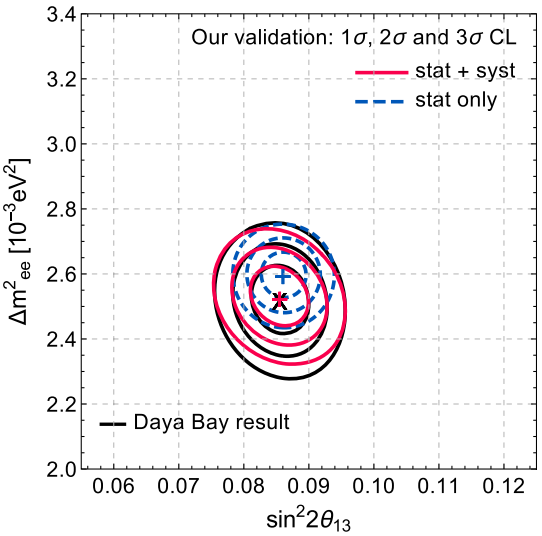

FIG. 4. Our validation on Δm^2_{ee} vs $\sin^2 2\theta_{13}$ fit using the Daya Bay data (1958 days), including systematics and statistics uncertainties in red solid lines, and including statistics only in blue dashed lines, for 1, 2 and 3σ allowed regions. The fit of the Daya Bay collaboration with 1958 days from [19] is represented in the solid black lines. The agreement between our analysis (solid red lines) and Daya Bay's analysis (solid black lines) is excellent.

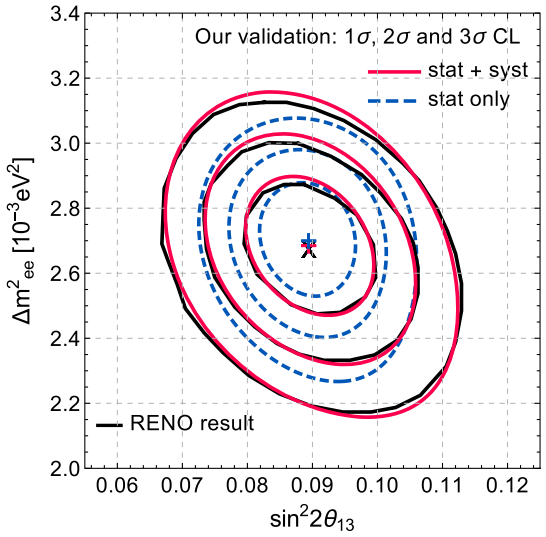

FIG. 5. Our validation on Δm^2_{ee} vs $\sin^2 2\theta_{13}$ fit using the RENO data (2200 days), including systematics and statistics uncertainties in red solid lines, and including statistics only in blue dashed lines, for 1, 2 and 3σ allowed regions. The fit of the RENO collaboration with 2,200 days from [20] is represented in the solid black lines. The agreement between our analysis (solid red lines) and RENO's analysis (solid black lines) is excellent.

the Δm^2_{ee} vs $\sin^2 2\theta_{13}$ from the Daya Bay and RENO collaborations as it is shown in Figs. 4, 5. The Daya Bay and RENO collaboration contours are taken from the Supplementary Material of [19] and from Fig. 3 of [20], respectively.

The agreement between our results and Daya Bay as well as RENO for the measurements of Δm^2_{ee} vs $\sin^2 2\theta_{13}$ is an excellent validation of the methods and numbers used in our analysis. Therefore, our constraint on Δm^2_{21}, using the publicly available data of Daya Bay and RENO, has a firm basis.

APPENDIX B: NUMBER OF EXPECTED EVENTS AND PULL PARAMETERS IN χ^2

The expected numbers of signal events in a detector d in a prompt energy bin i, X^d_i, is computed as follows up to a common input (e.g., reactor power, total number of protons) which cancels when taking ratios in the χ^2 computation.

$$X^d_i = \sum_r \sum_{\rm iso} \frac{a^d}{L^2_{rd}} \int_{E^{\rm rec}_i}^{E^{\rm rec}_{i+1}} {\rm d}E^{\rm rec} \int_0^\infty {\rm d}E_\nu \sigma(E_\nu) f^{\rm iso} \phi^{\rm iso}(E_\nu) \times P^{rd}_{\bar\nu_e\to\bar\nu_e}(E_\nu) R(E^{\rm rec}, E_\nu) \quad \text{(B1)}$$

where, the indices i, r, d, and iso refers to the ith energy bin, rth reactor, dth detector, and a fissionable isotope (^{235}U, ^{239}Pu, ^{238}U, or ^{241}Pu), respectively, and a^d is the detector efficiency. L_{rd} is the baseline between the reactor r and the detector d. E_ν and $E^{\rm rec}$ are the neutrino true energy and the reconstructed energy, both related by the detector response function $R(E^{\rm rec}, E_\nu)$. The $\sigma(E_\nu)$ is the IBD cross section computed performing the integral in $\mathrm{d}\cos\theta$ of the differential cross section in [22] and the $f^{\rm iso}$ is the averaged fission fraction[4] and the $\phi^{\rm iso}(E_\nu)$ is the Huber-Mueller flux prediction [23,24]. $P^{rd}_{\bar\nu_e\to\bar\nu_e}(E_\nu)$ is the oscillation probability from reactor r to detector d in the three neutrino oscillation paradigm.

The pull parameters accounting for detection efficiency (ϵ^d) and relative energy scale (η^d) are included in the number of expected events as follows

$$X^d_i(\epsilon^d, \eta^d) = \epsilon^d \sum_r \sum_{\rm iso} \frac{a^d}{L^2_{rd}} \int_{\eta^d E^{\rm rec}_i}^{\eta^d E^{\rm rec}_{i+1}} {\rm d}E^{\rm rec} \int_0^\infty {\rm d}E_\nu \times \sigma(E_\nu) f^{\rm iso} \phi^{\rm iso}(E_\nu) P^{rd}_{\bar\nu_e\to\bar\nu_e}(E_\nu) R(E^{\rm rec}, E_\nu).$$

For RENO, the efficiency pull parameter is included in the ratio.

The background pull parameters are included in background events B^d_i used in $D^{F/N}_i \equiv \frac{O^F_i - B^F_i}{O^N_i - B^N_i}$ as follows

$$B^d_i(b^d_{\rm LH}, b^d_{\rm acc}, b^d_{\rm n}) = B^d_i + (b^d_{\rm LH} - 1) B^d_{{\rm LH},i} + (b^d_{\rm acc} - 1) B^d_{{\rm acc},i} + (b^d_{\rm n} - 1) B^d_{{\rm n},i},$$

where B^d_i ($B^d_{{\rm LH},i}$, $B^d_{{\rm acc},i}$ and $B^d_{{\rm n},i}$) represents the number of total (Li-He, accidental and fast neutron) background events in the ith prompt energy bin in the dth detector, and the small b represents the corresponding pull parameter.

APPENDIX C: FIXED VS FREE Δm^2_{ee}

For the results in the main body of our paper we constrained Δm^2_{ee} treating it as a pull parameter using LBL experiments input. In this section we show the impact of Δm^2_{ee} fixed and set free. A 2-dimensional scan over Δm^2_{21} and $\sin^2 2\theta_{13}$ is performed to find the best fit value pair at the minimum value of χ^2 described earlier, where in the oscillation probability θ_{12} is fixed as $\sin^2\theta_{12} = 0.310$ but Δm^2_{ee} is set free within the range of $[1.55, 3.55] \times 10^{-3}$ eV^2. Results with a fixed $\Delta m^2_{ee} = 2.45 \times 10^{-3}$ eV^2 are also obtained and compared to those with Δm^2_{ee} set free. Figure 6, left and middle panels, shows the results of Δm^2_{ee} fixed and free for Daya Bay and RENO. It is observed that the effect of floating Δm^2_{ee} is bigger than adding systematic uncertainty for both Daya Bay and RENO. For floating Δm^2_{ee} case, the corresponding

[4]Ideally we would have the information on the fission factions as a function of time in each reactor, but since we do not have this information we take the same averaged values for all the detectors. This means that any systematic uncertainty on the flux predictions will cancel when taking ratios of the expected events in different experimental sites.

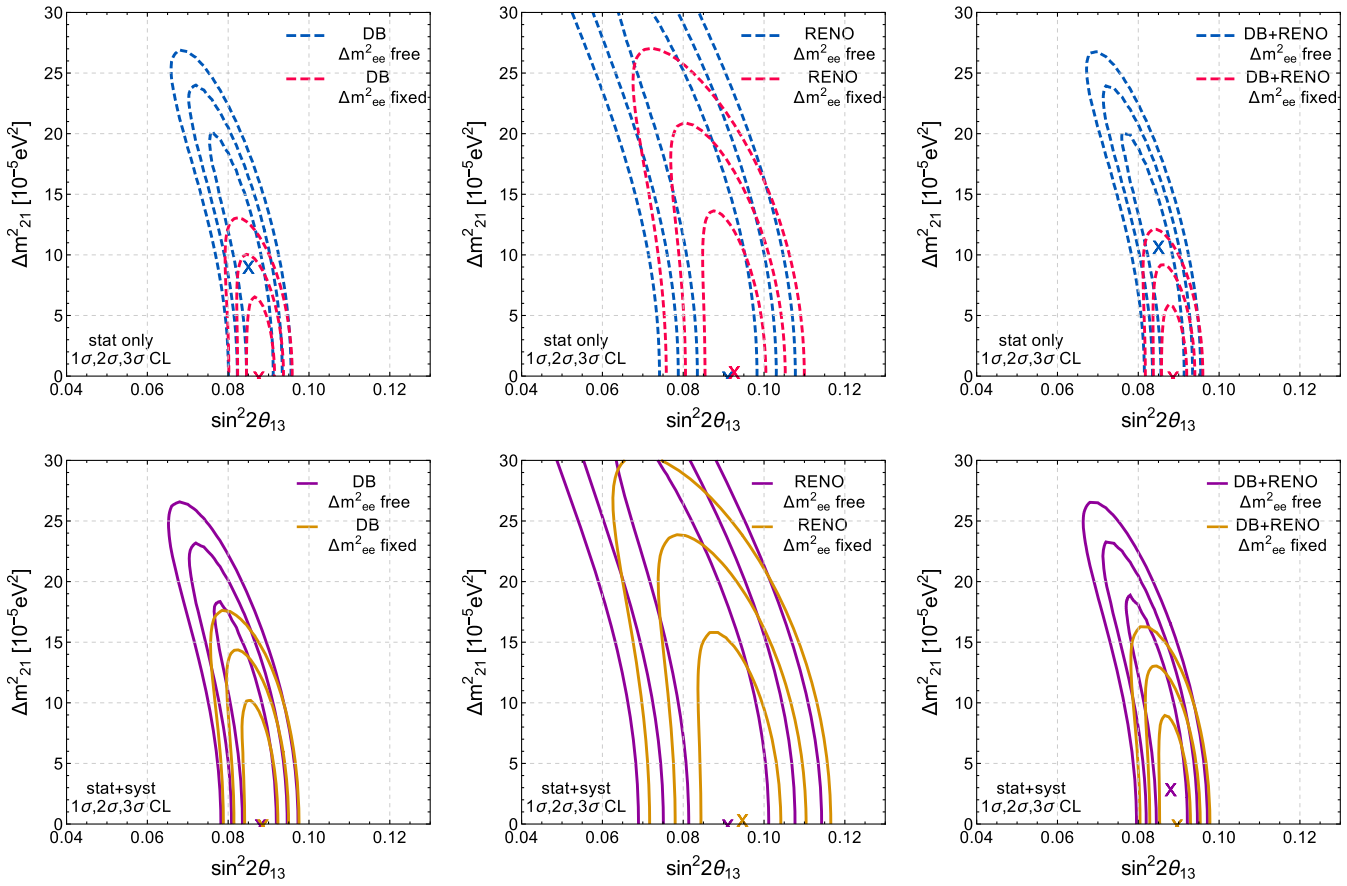

FIG. 6. Daya Bay (left panels), RENO (middle panels) and combined (right panels) 1, 2 and 3σ allowed regions in the Δm^2_{21} vs $\sin^2 2\theta_{13}$ parameter space, leaving Δm^2_{ee} free or fixed at 2.45×10^{-3} eV^2. For all panels, the dashed lines include only statistical uncertainties whereas the solid lines include both statistical and systematic uncertainties. The best fit values are shown with $\times$ signs. This figure demonstrates the extremes of our result to variation of Δm^2_{ee}.

Δm^2_{ee} values for the minimum χ^2 are found to be 2.50×10^{-3} eV^2 (2.68×10^{-3} eV^2) for Daya Bay (RENO) and it is within 1σ uncertainty of each of their measurements. Figure 6, right panels shows the results with combined analysis. For floating Δm^2_{ee} case, the corresponding Δm^2_{ee} value for the minimum χ^2 is found to be 2.54×10^{-3} eV^2 and it is within 1σ uncertainty of the Daya Bay best fit value, i.e., $[2.52 \pm 0.07] \times 10^{-3}$.

[1] S. H. Seo and S. J. Parke, Phys. Rev. D **99**, 033012 (2019).
[2] F. P. An *et al.* (Daya Bay Collaboration), Phys. Rev. Lett. **115**, 111802 (2015).
[3] J. H. Choi *et al.* (RENO Collaboration), Phys. Rev. Lett. **116**, 211801 (2016).
[4] K. Abe *et al.* (Super-Kamiokande Collaboration), Phys. Rev. D **83**, 052010 (2011).
[5] B. Aharmim *et al.* (SNO Collaboration), Phys. Rev. C **88**, 025501 (2013).
[6] A. Gando *et al.* (KamLAND Collaboration), Phys. Rev. D **83**, 052002 (2011).
[7] F. An *et al.* (JUNO Collaboration), J. Phys. G **43**, 030401 (2016).
[8] D. S. Ayres *et al.* (NOvA Collaboration), arXiv:hep-ex/0503053.
[9] K. Abe *et al.* (T2K Collaboration), Nucl. Instrum. Methods Phys. Res., Sect. A **659**, 106 (2011).
[10] I. Esteban, M. C. Gonzalez-Garcia, A. Hernandez-Cabezudo, M. Maltoni, and T. Schwetz, J. High Energy Phys. 01 (2019) 106.
[11] R. Acciarri *et al.* (DUNE Collaboration), arXiv:1512.06148.

[12] K. Abe *et al.* (Hyper-Kamiokande Proto- Collaboration), Prog. Theor. Exp. Phys. **2015**, 053C02 (2015).
[13] K. Abe *et al.* (Hyper-Kamiokande Collaboration), Prog. Theor. Exp. Phys. **2018**, 063C01 (2018).
[14] K. Abe *et al.* (T2K Collaboration), Phys. Rev. D **96**, 092006 (2017); **98**, 019902(E) (2018).
[15] K. Abe *et al.* (Hyper-Kamiokande Collaboration), arXiv: 1805.04163.
[16] F. Capozzi, S. W. Li, G. Zhu, and J. F. Beacom, Phys. Rev. Lett. **123**, 131803 (2019).
[17] H. Nunokawa, S. J. Parke, and R. Z. Funchal, Phys. Rev. D **72**, 013009 (2005).
[18] S. Parke, Phys. Rev. D **93**, 053008 (2016).
[19] D. Adey *et al.* (Daya Bay Collaboration), Phys. Rev. Lett. **121**, 241805 (2018).
[20] G. Bak *et al.* (RENO Collaboration), Phys. Rev. Lett. **121**, 201801 (2018).
[21] S. H. Seo (RENO Collaboration). AIP Conf. Proc. **1666**, 080002 (2015).
[22] P. Vogel and J. F. Beacom, Phys. Rev. D **60**, 053003 (1999).
[23] P. Huber, Phys. Rev. C **84**, 024617 (2011); **85**, 029901(E) (2012).
[24] T. A. Mueller *et al.*, Phys. Rev. C **83**, 054615 (2011).